Microwave magnetic resonance in amorphous GdAl films

J. P. Jamet* and A. P. Malozemoff
IBM Thomas J. Watson Research Center, Yorktown Heights, New York 10598
(Received 23 November 1977; revised manuscript received 9 March 1978)

The microwave absorption spectrum of amorphous sputtered Gd_xAl_{1-x} films at 9.13 GHz exhibits a single broad line which is studied as a function of temperature and composition x. In the paramagnetic regime, the g factor has a composition-independent positive shift of 0.006 ± 0.004 above 1.992 of the free Gd^{3+} ion, in contrast to negative shifts previously reported for crystalline GdAl. The shift is interpreted as arising from an exchange interaction J_{df} of the Gd f shell with electrons of d character. The g-shift contribution of the exchange interaction J_{sf} with s electrons is presumed to be hidden because of a "thermal bottleneck." This latter exchange interaction has a minimum value of 0.1 eV, as deduced from paramagnetic Curie temperatures. Using the observed temperature dependence of the resonance linewidth plus approximate band parameters from analogous dilute crystalline systems, the spin-lattice relaxation rate of amorphous Gd_xAl_{1-x} is estimated to be $10^{13}x$ Hz, in order-of-magnitude agreement with dilute crystalline systems. At lower temperatures the field for resonance shifts down, strongly for $x = 0.37$ but less strongly for higher Gd concentration. This shift is interpreted as an effective anisotropy field arising from local demagnetizing fields of an inhomogeneous (spin-glass) system. The composition dependence of the shift indicates that with increasing Gd concentration, the alloy becomes more magnetically homogeneous, gradually approaching simple ferromagnetism.

I. INTRODUCTION

We report here on a microwave magnetic-resonance study of amorphous intermetallic alloys Gd_xAl_{1-x} with $x = 0.37$, 0.56, and 0.81. Studies of this type have been done on the corresponding crystalline alloys,[1-5] and the results have given information about the magnetic structure, in particular about the couplings between localized moments and conduction electrons. The magnetic-resonance study of the amorphous GdAl alloy is particularly interesting because its previously determined properties differ so radically from the corresponding crystalline GdAl alloys. For example, magnetic measurements show that crystalline $GdAl_2$ is a ferromagnet while amorphous $GdAl_2$ exhibits spin-glass behavior, as first reported by Mizoguchi and co-workers.[6-8] More recent specific-heat measurements have indicated that in the spin-glass matrix, there is some degree of magnetic inhomogeneity arising from partially ferromagnetic clusters of dimension 35 Å.[9] Small-angle scattering measurements have also indicated structural inhomogeneities of comparable dimensions.[10]

In Sec. II, we describe experimental techniques and present results on the resonance curves, including their field position, shape, and linewidth. In Sec. III we correct for demagnetizing effects and extract the intrinsic g shifts and field shifts. Key differences with crystalline alloys are a small g shift of the opposite sign at high temperature and a huge line shift to lower fields at low temperatures. In Sec. IV we use the Ruderman-Kittel-Kasuya-Yosida (RKKY) theory to interpret the g shift and temperature dependence of the linewidth at temperatures well above the spin-glass ordering. We discover that the exchange interaction between the localized gadolinium moment and the conduction electrons appears to have the opposite sign from that in the crystalline counterparts. We attempt to relate these differences to the previously observed magnetic properties. In Sec. V we discuss the field shifts at low temperatures in terms of a local anisotropy field arising from a columnar magnetization distribution and strong exchange coupling. We describe a detailed model of this effect, which fills out the simplified version described in an earlier paper.[11]

II. EXPERIMENTAL TECHNIQUES AND RESULTS

The samples were prepared[6-8] by sputtering in argon from arc-melted targets onto high resistivity polished silicon substrates with a small substrate bias voltage (25–50 V). The purpose of the bias voltage was to reduce void structure which often appears in zero-bias sputtering, but the voltage was kept low to minimize structural anisotropy of the type that appears for example in GdCo bias-sputtered films. Thicknesses given in Table I were measured by Talysurf on samples where small areas were etched. The common method of masking a small area of the substrate during deposition was found less reliable for thickness measurement because the presence of the mask perturbs the film growth in its vicinity, leading often to an overestimate of the thickness.

TABLE I. Parameters of amorphous GdAl films.

Nominal composition (atom fraction X 100)	$Gd_{36}Al_{63}$	$Gd_{56}Al_{44}$	$Gd_{81}Al_{19}$
Gd	35	51	78
Al	58	40	19
Ar	3	9	3
Mo	4	...	...
h (μm)	3.7	2.4	2.0
E_F (eV)	9.5	8.7	7.9
Δg (± 0.004)	0.007	0.008	0.004
J_{sf} (Δg) (± 0.015 eV)	0.03	0.03	0.015
$d\Delta H/dT$ (Oe/K)	3.1	4	3.7
$\lvert\Delta g\rvert$(Korringa)	0.011	0.013	0.013
$\Theta(K)$	30	104	110
$\lvert J_{sf\min}\rvert$(eV)	0.11	0.16	0.14
$N(10^{22}\,\mathrm{cm}^{-3})$	4.1	3.4	3.1
$2\pi\Lambda_0$ (Å)	35	60	55

There was also considerable nonuniformity in thickness over the sample surface; so the thickness is only reliable to ±20%.

The three samples have nominal film compositions (metals only) of 0.37, 0.56, and 0.81 atom fraction Gd. We use these values to identify the samples and relate them to other papers. However the true film compositions were measured by electron microprobe and are given in Table I. In addition to Gd and Al, all samples have a significant amount of argon which dilutes the magnetic system. Some oxygen is also present but cannot be accurately determined from electron microprobe. It dilutes the system and is presumed to tie up a certain amount of Gd in Gd_2O_3. The small amount of Mo content in the first sample is a stray impurity. The third sample, with the highest Gd concentration, has been overcoated *in situ* after deposition with a 1-μm-thick layer of Si_3N_4 to avoid oxygen contamination which otherwise might occur after removal from the deposition chamber. We believe that oxygen contamination of the second sample is responsible for a resonance "surface mode" which will be discussed further below. The overcoating on the third sample reduced but did not eliminate evidence of a surface mode.

The microwave resonance data were taken using a standard Varian spectrometer at ~9 GHz (X band). The cavity had two holes to insert a helium-gas flow dewar. The temperature was controlled by manual regulation of the voltage across a small resistance heater inserted inside the tube.

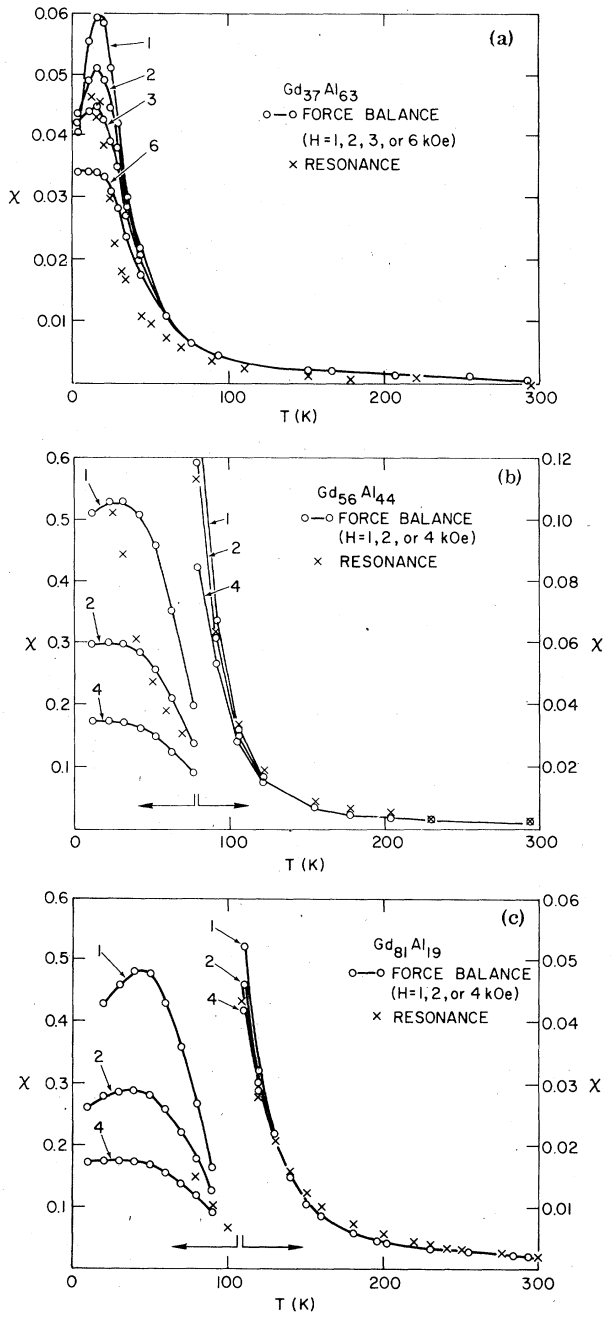

FIG. 1. Volume susceptibility χ vs temperature T of three amorphous GdAl films: (a) $Gd_{37}Al_{63}$, (b) $Gd_{56}Al_{44}$, and (c) $Gd_{81}Al_{19}$. Faraday force balance measurements represent M (at the indicated field H applied in the plane of the film) divided by H. Resonance measurements represent Eq.(3.7) of the text.

The samples of area ~1 × 5 mm² were attached with a small amount of vacuum grease to a quartz rod which could be inserted, rotated or removed during the experiment. The resonance spectrum

was measured for two orientations of the external dc magnetic field, perpendicular and parallel to the plane of the sample.

The magnetic properties of the films were measured previously by a Faraday force balance,[6-8] and Fig. 1 shows some of the results for the volume susceptibility $\chi = M/H$ determined with the applied field H in the plane of the sample. The uncertainty in thickness mentioned earlier, coupled with the problems of accurate subtraction of substrate contributions, limits the absolute accuracy of the magnetic measurements to about 30%. At high temperatures the susceptibility follows a Curie-Weiss law and the paramagnetic Curie temperatures Θ are given in Table I. At lower temperatures there are susceptibility maxima which become most pronounced for the sample with least Gd (see Fig. 1). Since these susceptibilities are determined with the applied field in the plane of the sample, the downturn in susceptibility at low temperatures is not likely to be a shape demagnetizing effect. Nor is it likely to be an anisotropy effect since Gd is believed to be an S-state ion with negligible single-ion anisotropy or anisotropy of exchange. As discussed elsewhere,[6-8] the most likely explanation is that these samples show some degree of spin-glass behavior, although the samples with higher Gd concentration are predominantly ferromagnetic.

Some typical resonance curves, representing the conventional field derivative of the absorptive component of the microwave susceptibility, are shown in Fig. 2. The curves have fairly large linewidths and are asymmetric. In many cases reported in the literature,[3-5,12] such asymmetry arises from the complex metallic impedance which exists when the electromagnetic penetration length is less than the sample dimension. Our samples have thickness of 2–4 μm. The penetration length $(2\rho/\omega\mu)^{1/2}$ can be estimated to be 8 μm, assuming an angular frequency $\omega = 2\pi \times 9$ GHz, and a resistivity $\rho = 200$ $\mu\Omega$ cm, and provided we assume the permittivity of free space $\mu = 4\pi \times 10^{-7}$ henry/m. In fact the permittivity should be larger because of the unsaturated nature of our specimens, and therefore the penetration depth should be smaller. We follow the conventional approach[3-5,12] in analyzing the curves $F(x)$ as a superposition of the derivative of the real and imaginary parts of a Lorentzian:

$$F(x) = A(1 - ax - x^2)/(1 + x^2)^2 , \tag{2.1}$$

$$x = (H - H_0)/\Delta H . \tag{2.2}$$

Here A and a are fitting parameters, H is the applied field, H_0 is the "true" line center and ΔH is the half-power half-width of the absorption part of the resonance line. Henceforth, when H is applied in the film plane, we call the true line center $H_{\parallel}$ and the linewidth $\Delta H_{\parallel}$. When H is normal to the film plane, we call them $H_{\perp}$ and $\Delta H_{\perp}$, respectively.

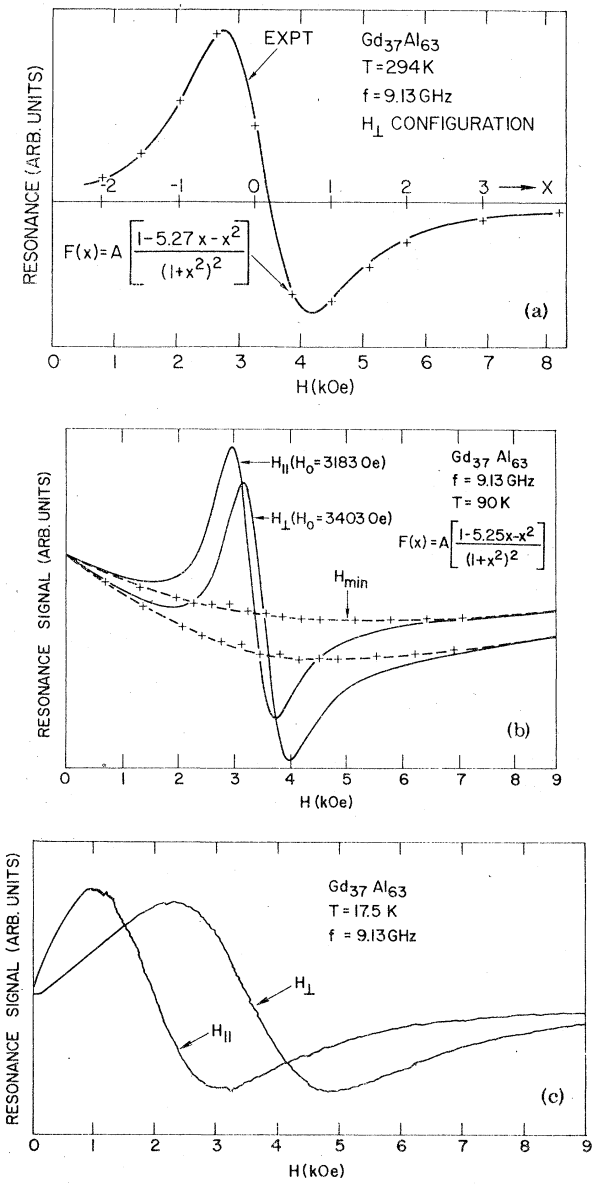

FIG. 2. Resonance signals, i.e., field derivatives of the absorptive component of the rf susceptibility, at 9.13 GHz for $Gd_{37}Al_{63}$ at (a) 294 K, (b) 90 K, and (c) 17.5 K. In (a) the solid line is the experimental result and the crosses are the Lorentzian line shape fit $F(x)$ [see Eqs. (2.1) and (2.2)]. In (b) the crosses represent the difference between the solid experimental curves and the $F(x)$ fit.

An example of the fit of Eq. (2.1) to the data is shown by the crosses in Fig. 2(a). Such results were obtained for $Gd_{37}Al_{63}$ above 200 K, for

$Gd_{56}Al_{44}$ above 30 K except for a shoulder in the $H_\perp$ curve below 110 K, and for $Gd_{81}Al_{19}$ above 60 K. Figure 2(c) shows resonance curves at lower temperature, where a large offset develops between $H_\perp$ and $H_\parallel$. In an intermediate temperature range, as shown in Fig. 2(b), one can see that there exists an apparent curved baseline. The minimum is indicated by H_{min}. This effect is relatively important below 200 K for $Gd_{37}Al_{63}$. It might possibly be interpreted as a secondary resonance mode with a very large linewidth. The resonant cavity gives a linear polarization, which

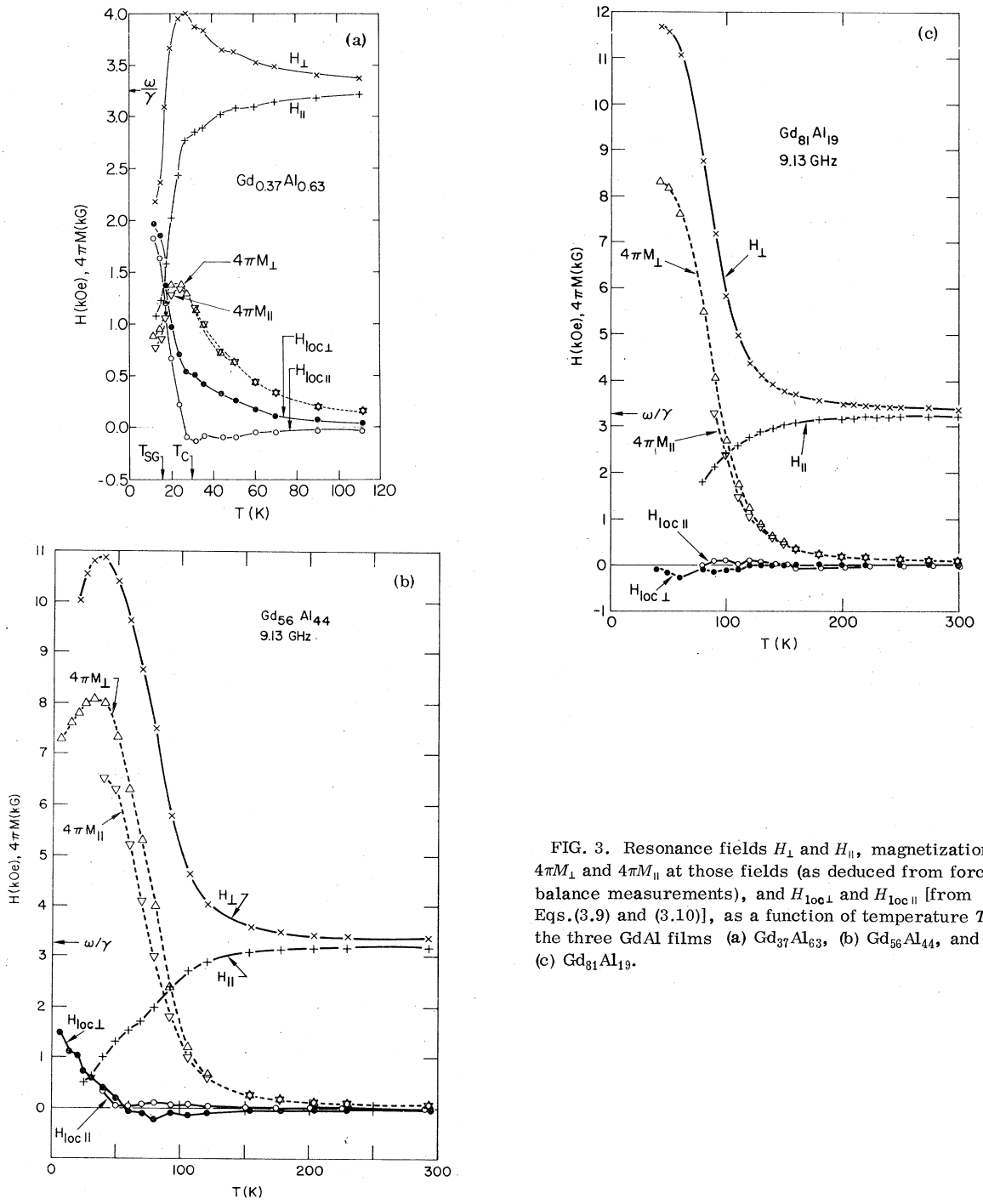

FIG. 3. Resonance fields $H_\perp$ and $H_\parallel$, magnetizations $4\pi M_\perp$ and $4\pi M_\parallel$ at those fields (as deduced from force balance measurements), and $H_{loc\perp}$ and $H_{loc\parallel}$ [from Eqs.(3.9) and (3.10)], as a function of temperature T in the three GdAl films (a) $Gd_{37}Al_{63}$, (b) $Gd_{56}Al_{44}$, and (c) $Gd_{81}Al_{19}$.

means that for the positive values of the magnetic field which we apply, we can get a superposition of the right circularly polarized mode and of the tail of the left one which occurs for the negative field values. The admixture of these two opposite modes becomes very important if the center of each mode occurs at field values smaller than or equal to the half linewidth. A precise determination of the resonance field of the second mode is very difficult in this case, but one can make a rough evaluation of the temperature dependence of the linewidth, which is 45 ± 10 Oe/K for $50 < T < 200$ K. This value is much larger than the value obtained for the main mode (see below), which suggests that some additional relaxation mechanism is involved. We speculate that one possibility for such relaxation is surface relaxation; another involves different regions of the sample as suggested by the inhomogeneity or cluster picture of Sec. V. We have not investigated this mode in any more detail and attempt no further interpretation.

The values of $H_{\parallel}$ or $H_{\perp}$ determined in the fit using Eqs. (2.1) and (2.2) are plotted in Fig. 3 for the three samples. The perpendicular resonance is always shifted to higher fields than the parallel one, because of a demagnetizing effect which will be considered further in Sec. III. In addition there is a dramatic shift of both resonances to lower fields in $Gd_{37}Al_{63}$ below the paramagnetic Curie temperature. There is a relatively small such shift in $Gd_{56}Al_{44}$. The shift is not observable in $Gd_{81}Al_{19}$ although a shift cannot be ruled out since remanence effects (see below) prevent accurate determination of the resonance fields below 40 K.

ΔH is plotted for the parallel and perpendicular field configuration in Fig. 4. The linewidth decreases roughly linearly with decreasing temperature at high temperatures, and the rate of change $d\Delta H/dT$ is given in Table I. At low temperatures approaching the paramagnetic Curie temperature, the linewidth increases once again with a roughly inverse temperature dependence. It is interesting to note that for $Gd_{37}Al_{63}$, one finds within experimental error $\Delta H_{\parallel}/\Delta H_{\perp} = H_{\parallel}/H_{\perp}$. A special complication occurs in $Gd_{56}Al_{44}$ where there is evidence for an extra resonance appearing as a shoulder in the $H_{\perp}$ spectrum below about 150 K. The presence of this shoulder complicates the determination of the linewidth of the main line, and there is accordingly a noticeable anomaly in Fig. 4(b). Such a shoulder could arise from a surface layer with altered properties, for instance due to oxidation. An attempt was made to avoid such an effect in $Gd_{81}Al_{19}$ by overcoating with a protective layer. While there was no evidence of a shoulder, there is still an anomaly in $\Delta H_{\perp}$ [Fig. 4(c)]. Apparently the overcoating was unsuccessful in eliminating all surface layers, but the effect has not been investigated further. Below 60 °K the curves become distorted from the shape of Eq. (2.1) and only approximate values of ΔH and H_0 can be determined.

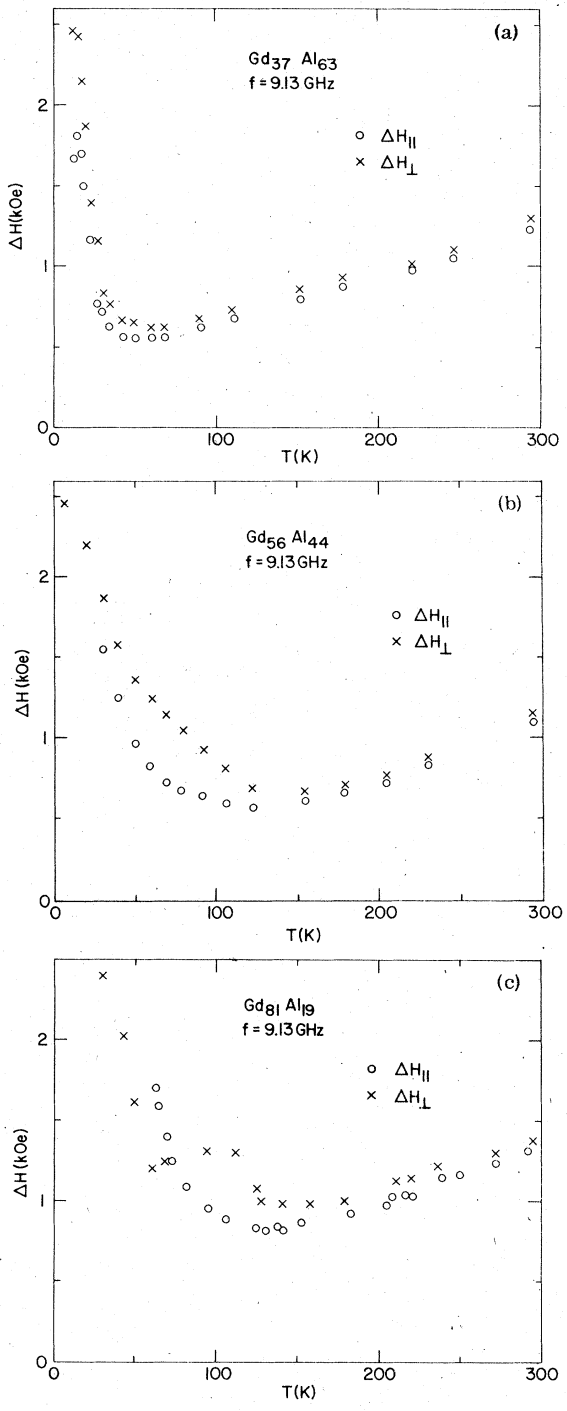

FIG. 4. Resonance linewidths ΔH as deduced from Eqs. (2.1) and (2.2) vs temperature T for the three GdAl films.

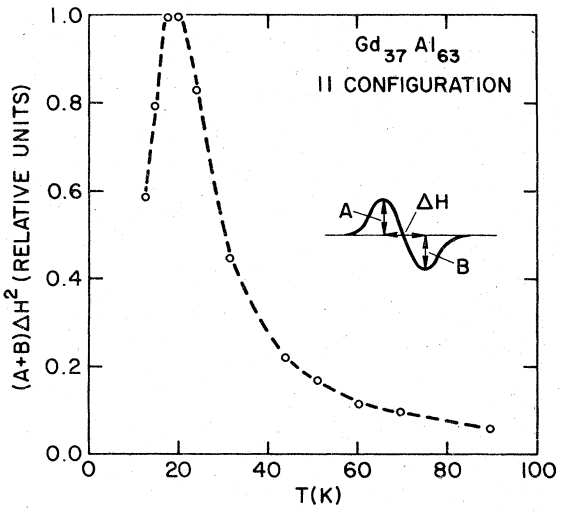

FIG. 5. Relative resonance line intensity $\Delta H^2(A+B)$ (see insert) vs temperature for the $H_{\parallel}$ configuration in $Gd_{37}Al_{63}$.

The area under the resonance absorption curve can be shown to be proportional to $(A+B)\Delta H^2$, where A and B are the amplitudes of the positive and negative peaks of the derivative signal and ΔH is the field difference between them, as illustrated in the insert to Fig. 5. The relative area is plotted in Fig. 5 for the $Gd_{37}Al_{63}$ sample and shows a peak in the vicinity of the susceptibility maximum. A complication in the determination of the resonance curves is illustrated in Fig. 6. The position of the resonances at low temperature depends on the history of the field- and temperature-dependence of the sample. While an extensive study of these properties was not undertaken, a rough measure of the isothermal remanence was obtained by measuring the difference δH_a in peak positions with fields increasing from zero or decreasing from ~14 kG in the film plane.

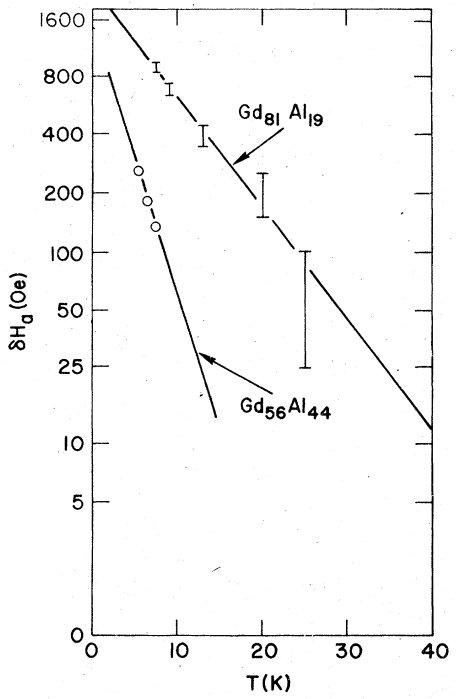

FIG. 6. Isothermal remanence δH_a of resonance line position as a function of temperature. δH_a was determined as the difference between the line position sweeping up from zero field down from 14 kG.

III. DETERMINATION OF g FACTORS AND LOCAL ANISOTROPY FIELDS

In this section we give a phenomenological description of the temperature-dependent resonance fields $H_{\parallel}$ and $H_{\perp}$ for the parallel and perpendicular configurations, respectively. The analysis allows us to extract the g factors and effective local anisotropy fields from the data. We discuss the microscopic origins of these effects in later sections.

The primary features of $H_{\parallel}$ and $H_{\perp}$ are that $H_{\perp} - H_{\parallel}$ increases as temperature decreases and that as the freezing temperature of the spin glass is approached, both fields shift strongly downward. The increase of $H_{\perp} - H_{\parallel}$ is a well-known characteristic of paramagnetic or magnetic films and may be understood in the following way: For a material of volume susceptibility χ, the magnetizations induced by applied fields $H_{\parallel}$ and $H_{\perp}$ parallel and perpendicular to the film plane are

$$M_{\parallel} = \chi H_{\parallel}\,, \tag{3.1}$$

$$M_{\perp} = \chi(1+4\pi\chi)^{-1}H_{\perp}\,. \tag{3.2}$$

The well-known resonance equations for the parallel and perpendicular configurations are

$$\omega\gamma^{-1} = [H_{\parallel}(H_{\parallel}+4\pi M_{\parallel})]^{1/2}\,, \tag{3.3}$$

$$\omega\gamma^{-1} = H_{\perp} - 4\pi M_{\perp}\,, \tag{3.4}$$

where $\omega = 2\pi f$, f is the microwave frequency, $\gamma = 2\pi g\mu_{\beta}/h$ is the gyromagnetic ratio, g is the g factor, μ_{β} is the Bohr magneton, and h is Planck's constant. Substituting Eqs. (3.1) and (3.2) in (3.3) and (3.4), one finds for the parallel and perpendicular equations

$$\omega\gamma^{-1} = H_{\perp}(1+4\pi\chi)^{-1}\,, \tag{3.5}$$

$$\omega\gamma^{-1} = H_{\parallel}(1+4\pi\chi)^{1/2}\,, \tag{3.6}$$

which may be solved to give

$$\chi = (4\pi)^{-1}[(H_{\perp}H_{\parallel}^{-1})^{2/3} - 1]\,, \tag{3.7}$$

$$g_{\text{eff}} = 714.5\, f H_{\perp}^{-1/3} H_{\parallel}^{-2/3}\,, \tag{3.8}$$

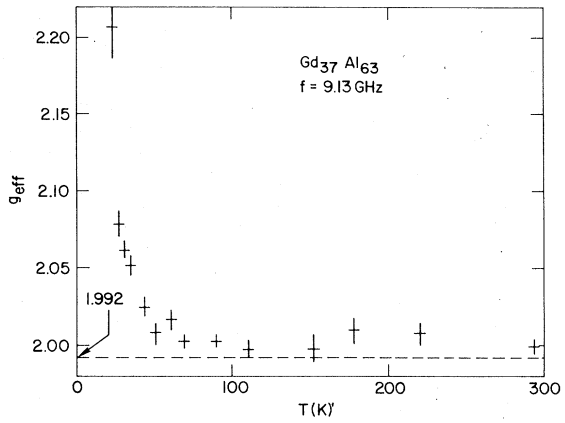

FIG. 7. Effective g factors, according to Eq.(3.8) of the text, vs temperature T, for the sample $Gd_{37}Al_{63}$. Dashed line shows expected g factor of 1.992 for the free Gd^{3+} ion.

for f in GHz. Equation (3.7) shows that the difference between $H_\perp$ and $H_\parallel$ is related to a nonzero susceptibility χ.

Application of Eq. (3.7) to the resonance data gives the results shown as crosses in Fig. 1. Above about 100 K, the χ deduced from resonance agrees within 50% with that deduced from magnetic measurements. This agreement is considered reasonable because of the large error in the absolute magnetization measurement. At lower temperatures agreement is not expected because Eq. (3.7) breaks down due to the appearance of a nonlinear magnetization curve and local anisotropy fields (see below).

The g factors deduced from Eq. (3.8) are shown for $Gd_{37}Al_{63}$ in Fig. 7. Similar results are obtained for the other samples. The results indicate that at high temperatures g is essentially constant for all three samples and has a value close to the free-ion value[13] of 1.992. However on the average there is a small shift to higher g values. In Table I we give this g shift as determined at room temperature where the operating stability was greatest, for the determination requires measurement of peak positions to within a few oersteds. Of course, the quoted values also depend sensitively on our use of the formalism of Eqs. (2.1) and (2.2) to extract $H_\perp$ and $H_\parallel$. Within experimental accuracy, Δg is the same for all three films. We will return to a discussion of the physical significance of Δg in Sec. IV. The g shift appears to be essentially temperature independent until at lower temperatures the g values begin to deviate strongly upwards, as shown in Fig. 7. For reasons to be discussed at the end of Sec. IV, we consider these stronger g shifts to arise from a breakdown of Eqs. (3.7) and (3.8).

One reason for this breakdown is that at low temperatures the magnetization curve is no longer linear with field, as shown by the dependence of $\chi = M/H$ on the field H in Fig. 1. In addition there is the possibility of effective anisotropy fields arising from the local dipolar field. Calling the effective anisotropy field H_{loc} and assuming it acts in the direction of the applied dc field H, we may generalize the conventional resonance equations (3.3) and (3.4) to

$$\omega\gamma^{-1} = [(H_\parallel + H_{loc\parallel})(H_\parallel + H_{loc\parallel} + 4\pi M_\parallel)]^{1/2}, \quad (3.9)$$

$$\omega\gamma^{-1} = H_\perp + H_{loc\perp} - 4\pi M_\perp . \quad (3.10)$$

Here $M_\parallel$ and $M_\perp$ are taken to be the induced magnetization at the resonance fields $H_\parallel$ and $H_\perp$, respectively, and $H_{loc\parallel}$ and $H_{loc\perp}$ are the effective anisotropy fields in the parallel and perpendicular configurations, respectively. We return to an interpretation of these anisotropy fields in Sec. V, and here we simply treat them on a phenomenological basis. In Fig. 3 are shown $M_\parallel$ and $M_\perp$ deduced from magnetic measurements, as well as $H_{loc\perp}$ and $H_{loc\parallel}$ from Eqs. (3.9) and (3.10), assuming $g = 2$ independent of temperature. In $Gd_{37}Al_{63}$, $H_{loc\perp}$ gradually increases with decreasing temperature, and below the paramagnetic Curie temperature both $H_{loc\parallel}$ and $H_{loc\perp}$ increase strongly. In $Gd_{56}Al_{44}$ this tendency is slightly evident but is absent altogether in $Gd_{81}Al_{19}$.

IV. INTERPRETATION OF HIGH-TEMPERATURE BEHAVIOR

Because of the well-defined magnetic state of Gd and because of the well-shielded nature of its $4f$ electrons, direct exchange between Gd ions is unlikely. It is common in metallic systems containing localized moments to consider the dominant exchange interaction to arise from the indirect interaction via the conduction electrons, which is called the RKKY interaction. In this section we apply the RKKY theory[14-17] to the interpretation of our results.

The RKKY interaction is given by the formulas

$$E_{ij} = -2J_{ij}\vec{S}_i \cdot \vec{S}_j , \quad (4.1)$$

$$J_{ij} = \tfrac{9}{8}\pi n_0^2 E_F^{-1} J_{sf}^2 F(2k_F r_{ij}) , \quad (4.2)$$

$$F(q) = q^{-4}(\sin q - q\cos q) . \quad (4.3)$$

Here $\vec{S}_i$ is the spin vector of the ith Gd atom, E_{ij} is the interaction energy between the ith and the jth atoms, J_{ij} is the effective exchange interaction between these atoms, r_{ij} is the distance between the atoms, n_0 is the number of conduction electrons per atom, J_{sf} is the $q = 0$ component of the Fourier transform of the interaction integral between a localized-electron spin $\vec{S}$ and a conduction-electron

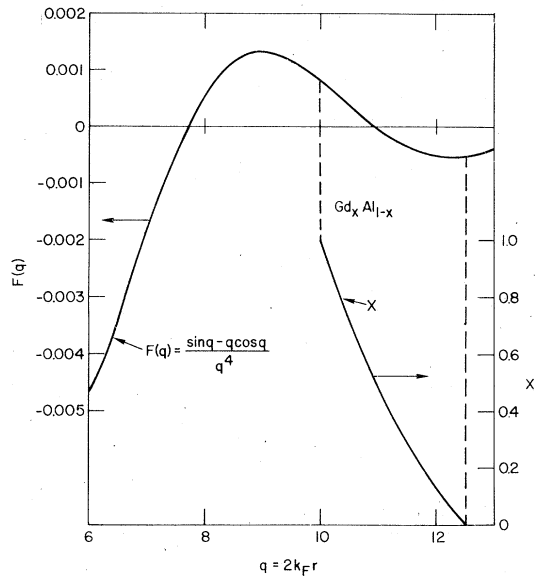

FIG. 8. RKKY function $F(q)$ [Eq.(4.3)] and the Gd atom fraction x [Eq.(4.5)] as a function of $q = 2k_F r$ in $Gd_x Al_{1-x}$. (After Mizoguchi, see Ref. 8.)

spin $\vec{s}$ (defined by the approximate Hamiltonian $\mathcal{H} = -J_{sf}\vec{S}\cdot\vec{s}$), E_F is the Fermi energy, and k_F is the Fermi wave vector. A plot of the function $F(2k_F r_{ij})$ is shown in Fig. 8. As is well known the function oscillates, giving ferromagnetic interactions between atoms placed with $r_{ij} < 4.5/2k_F$, antiferromagnetic interactions between atoms at $4.5/2k_F < r_{ij} < 7.7/2k_F$, ferromagnetic interactions between atoms at $7.7/2k_F < r_{ij} < 10.9/2k_F$, etc.

The oscillating interaction is damped above and beyond the falloff given in Eqs. (4.2) and (4.3) by electron relaxation caused by the finite electron mean free path. In our amorphous materials, with a resistivity of about 200 $\mu\Omega$ cm, the mean free path is only about a nearest-neighbor distance; so only nearest-neighbor interactions are presumed to be of importance. Mizoguchi *et al.*[6-8] have estimated the value of $q = 2k_F r_n$ assuming the Gd-Gd nearest-neighbor distance $r_n = 3.6$ Å for Gd and a simple free-electron picture with $n_0 = 3$. Assuming the atomic volumes $v_{Gd} = 33$ Å^3 for Gd and $v_{Al} = 16.6$ Å^3 for Al, one takes the average atomic volume v_a for $Gd_x Al_{1-x}$ to be a linear interpolation between these endpoints. Since

$$k_F = 2\pi(3n_0/8\pi v_a)^{1/3}, \tag{4.4}$$

one finds

$$x = [(3n_0/8\pi)(4\pi r/q)^3 - v_{Al}]/(v_{Gd} - v_{Al}). \tag{4.5}$$

This relationship is plotted in Fig. 8. It indicates that $q = 2k_F r$ for GdAl falls in the range from 10 to 12.5, spanning the second zero of the RKKY oscillation. The possibility of a spread in the nearest-neighbor distances arising from the amorphous structure implies the possibility of both ferromagnetic and antiferromagnetic exchange interactions as $q = 2k_F r_{ij}$ varies above or below 10.9. It is in this way that Mizoguchi *et al.*[6-8] have rationalized the occurrence of spin glass behavior in amorphous GdAl and the trend to ferromagnetism with increasing Gd concentration.

In fact the paramagnetic Curie temperatures Θ of all three samples are strongly positive. Since Θ is in theory proportional to the sum of *all* exchange interactions, ferromagnetic interactions must predominate in each sample. By contrast Fig. 8 suggests that below about $x = 0.55$, GdAl should be predominantly antiferromagnetic. To rationalize this discrepancy within the framework of the free-election model, one can invoke a mere 20% drop in electron concentration, which would shift the $x(q)$ curve by about one unit of q to the left.

The maximum possible ferromagnetic interaction in this range of $F(q)$ occurs at $q = 9$ where $F(q) = 0.0013$. Assuming nearest-neighbor interactions only and a molecular-field model, the paramagnetic Curie temperature is

$$\Theta \simeq 2S(S+1)zxJ_{ij}/3k, \tag{4.6}$$

where S is the Gd spin value ($\frac{7}{2}$), z is the number of nearest neighbors (~12), x is the atom fraction of Gd and J_{ij} is the average nearest-neighbor exchange. Thus a minimum value for J_{sf} can be determined from Eqs. (4.2) and (4.6) by taking the maximum value for $F(q)$. Using the free-electron mass to determine

$$E_F = (h^2/2m)(3n_0/8\pi v_a)^{2/3}, \tag{4.7}$$

we find E_F and $J_{sf\,min}$ as given in Table I.

The result for $J_{sf\,min}$ in the $Gd_{37}Al_{63}$ sample is supported by specific-heat measurements of Coey *et al.*,[9] who give a spin wave stiffness coefficient $D = 6.6 \times 10^{-31}$ erg cm^2 defined as $E = Dk^2$, where k is the wave vector of the spin wave. Using an earlier calculation[18] of the micromagnetic exchange stiffness A, one finds D given by

$$D = (\tfrac{1}{3})J_{ij}Szxr_{ij}^2. \tag{4.8}$$

Determining a minimum J_{sf} from (4.2) and (4.8), one finds a result within 5% of $J_{sf\,min}$ in Table I. The good agreement is merely a reflection of the good agreement between D and Θ previously referred to by Coey *et al.*[9]

The results for $J_{sf\,min}$ in amorphous GdAl may also be compared to results of magnetic measurements on other amorphous Gd systems,[7,20-23] including GdCu, GdAg, GdAu, and GdNi. As pointed

out recently by Heiman and Kazama[23] (see their Fig. 2), the ordering temperatures of all these systems are broadly consistent, rising roughly linearly with Gd concentration above about $x = 0.3$. (We note however that if the results of McGuire *et al.*,[7] Hauser,[20] and Boucher[21] are included on Heiman and Kazama's plot, the scatter at any given Gd concentration can reach a factor of 3.) This rough consistency means that if we use a nearest-neighbor mean-field analysis like the one we used above, we will find similar $J_{sf\,\min}$ values for all these systems, independent of Gd concentration. For example, using a similar method, Poon and Durand[19] determined $J_{sf} = 0.19$ eV in amorphous $Gd_{80}Au_{20}$, consistent with our $J_{sf\,\min}$ in Table I. Such values in the range of $J_{sf} = 0.2$ eV are also roughly consistent with values observed in crystalline systems. For example, $J_{sf} = 0.16$ in Gd metal[17] and 0.45 eV in crystalline $GdAl_2$.[2] Doubt about our assumption of nearest-neighbor interactions has been raised recently by the measurement of RKKY interactions in a dilute system, amorphous $La_{80}Au_{20}$:Gd.[24] From measurements of the approach to magnetic saturation, values of J_{sf} within 50% of those for amorphous $Gd_{80}Au_{20}$ were found. In summary, the question of the range of the RKKY interaction in amorphous materials has not yet been resolved, but for the purposes of further discussion and for comparison with spin resonance, we tentatively take $J_{sf} \sim 0.2$ eV as a rough value indicated by magnetic measurements.

Next we apply the RKKY theory to the interpretation of the "high-temperature" spin-resonance results. By "high-temperature" we refer to the temperature range in which Δg is essentially constant (e.g. above 70 K in Fig. 7) and in which ΔH increases linearly with T (e.g., above 70 K in Fig. 4(a)). The simplest RKKY theory implies a g shift according to the formula[16]

$$\Delta g = 3n_0 J_{sf}/4E_F = J_{sf}\eta_s\,, \tag{4.9}$$

where η_s is the s-electron density of states per atom per spin direction. (We note that this formula differs by a factor of 2 from Yosida's original result merely because Yosida defined J_{sf} in terms of the Hamiltonian $\mathcal{H} = -2J_{sf}\vec{S}\cdot\vec{s}$, instead of the currently more widespread convention that we use, namely, $\mathcal{H} = -J_{sf}\vec{S}\cdot\vec{s}$.) Using the observed g shifts, we deduce the positive J_{sf} values shown in Table I. Within the admittedly large experimental error, there is no significant shift in J_{sf} with composition. The Korringa relation[25]

$$d\Delta H/dT = \pi(\Delta g)^2 k/g\mu_\beta \tag{4.10}$$

relates the rate of change of linewidth [defined as in Eq. (2.2)] with temperature to the g shift. Using the observed $d\Delta H/dT$, we calculate Δg values close to but slightly larger than those observed directly (see Table I).

If we ignore the slight discrepancy between these two values for Δg and if we compare the $J_{sf\Delta g}$ deduced from these values to $J_{sf\,\min}$ deduced from Θ as discussed above, we find a large discrepancy of at least a factor of from 4 to 10 (see Table I). Within the context of the simple RKKY model, possible sources for this discrepancy could reside in our choices of 3 for n_0 and of the free-electron mass for m. However values from 16 to 100 times smaller ($J^2_{sf\Delta g}/J^2_{sf\,\min}$) for either of these parameters would be required to explain the discrepancy.

A similar difficulty emerges from the results of the only other comparable spin-resonance study of which we are aware, namely, a study of amorphous GdAg by Charles *et al.*,[26] although in this study there are serious complications due to the presence of crystalline phases. Nevertheless, just as we do, they find rough agreement between g shifts and the simple Korringa relation. Furthermore, if we assume a free-electron model, we deduce J_{sf} values from their observed g shifts which are in most cases significantly smaller than the values mentioned earlier from magnetic measurements.

A possible origin of the discrepancy may lie in the wave-vector dependence of the sf exchange interaction. Davidov *et al.*[27] have proposed a partial-wave expansion for $J_{sf}(q)$ and have given generalized formulas for Δg, $d\Delta H/dT$, and $J_{ij}(r_{ij})$, in terms of the parameters J^0, J^1, J^2, etc. which correspond to the coefficients of the partial-wave expansion. For Gd^{3+} they argue that all these parameters are likely to be positive and the lowest-order terms dominant. In this case and for $2k_F r_{ij} > 10$, it can be shown that the apparent net J_{sf} from magnetic measurements [their Eq. (9)] will be *smaller* than J_{sf} from spin resonance [their Eq. (2)]. But our results indicate the opposite. Thus the partial-wave idea cannot explain the discrepancy. In what follows we assume only the first partial wave is significant and this leaves our previous formulas [Eqs. (4.2) and (4.9)] unchanged (i.e., $J^0 \equiv J_{sf}$).

A more likely possibility to explain the discrepancy comes from another model proposed by Davidov *et al.*[28] to account for resonance results in $Gd_xLa_{1-x}Al_2$ intermetallic crystals. These authors considered several additional effects to extend the RKKY theory. First they considered the possibility that the conduction bands have both s and d character and can give rise to separate contributions to the g shift (Δg_s and Δg_d) and to the relaxation. Second, they included "thermal bottlenecking," which occurs when the relaxation rate

δ_{sL} of the conduction electrons to the lattice is smaller than their relaxation rate δ_{sf} to the magnetic f shell of the Gd ions, that is, when the quantity $\xi = \delta_{sL}/\delta_{sf}$ is small. Such an effect reduces both the resonance linewidth and the g shift. Davidov *et al.* further assumed that such a bottlenecking effect could be present for s electrons but could be ignored for d electrons because of their more rapid spin-lattice relaxation. Third, they included the effect of electron-electron interactions in terms of the "enhancement factors" α_s, α_d, $K_s(\alpha_s)$, and $K_d(\alpha_d)$, as defined by Narath and Weaver[29] or Shaw and Warren,[30] which lie between 0 and 1. In addition they included a factor $F_d(<1)$ which accounts for d-level degeneracy at the Fermi energy. They also considered so-called "dynamic effects," but we ignore these here since they are only relevant when the g shift is temperature dependent.[31]

Given the above assumptions one can write the following equations for the g shift Δg and the temperature derivative $d\Delta H/dT$ of the linewidth:[28]

$$\Delta g = \Delta g_d + \Delta g_s[\xi^2/(1+\xi)^2]\,, \tag{4.11}$$

$$\frac{d\Delta H}{dT} = \pi k g^{-1}\mu_\beta^{-1}\left[(\Delta g_d)^2 F_d K_d + (\Delta g_s)^2 K_s\left(\frac{\xi}{1+\xi}\right)\right]. \tag{4.12}$$

In applying these equations to an amorphous material, we first note that Eq. (4.12) contains no cross terms in the relaxation between s and d electrons, which is valid in cubic symmetry[28] but invalid in the lower symmetry amorphous structure. Since no theory is available at present for these cross terms, we ignore them and use Eq. (4.12) as it stands, recognizing the uncertainty this assumption introduces into the following analysis.

We can immediately see from the form of Eqs. (4.11) and (4.12) how the discrepancies we mentioned earlier can be resolved. If the s electrons are bottlenecked, the Δg we observe is primarily due to Δg_d, which could be considerably smaller than Δg_s. The large values of $J_{sf\,\min}$ in Table I would then be interpreted as arising primarily from sf interactions. The discrepancy between the two values of Δg in Table I can also be explained by arguing that if $\xi = \delta_{sL}/\delta_{sf}$ is sufficiently small, the Δg_s term in Eq. (4.11) is negligible while the corresponding term in Eq. (4.12) is not.

To make these possibilities more concrete, we avail ourselves of data taken on three crystalline systems,[28,32,33] $LaAl_2$, YAl_2, and $LuAl_2$ with dilute Gd impurities. These systems show unbottlenecked g shifts $\Delta g_s = 0.09 \pm 0.02$ and unbottlenecked $d\Delta H/dT$ values of 60 ± 20 Oe/K. The enhancement factors are roughly $\alpha_s = 0.6$ and $K_s(\alpha_s) = 0.45$. Further, from comparison of specific-heat measurements on $LaAl_2$ and YAl_2, Davidov *et al.*[28] have deduced the density of s states to be $\eta_s = 0.35$ states per eV per atom per spin. However a recent reinterpretation of these systems by Chock *et al.*[34] uses unpublished band calculations to deduce $\eta_s \sim 0.06$ states per eV per atom per spin, a value 5 times less than the former.

Davidov's value for the density of s states of these crystalline systems is within 50% of the free-electron result, suggesting that the s bands are approximately free-electron-like. It is then plausible to imagine that the various s-band parameters, including the density of s states, the enhancement factors and the sf exchange interaction, do not change significantly (e.g., by more than 50%) in going from the crystalline to the amorphous state. Thus, assuming that $\alpha_s = 0.6$, $K_s(\alpha_s) = 0.45$, and $\Delta g_s = 0.09$ for the amorphous system, we can solve Eqs. (4.11) and (4.12) for Δg_d and ξ, using our observed averaged values of $\Delta g = 0.006$ and $d\Delta H/dT = 3.6$ Oe/K from Table I. We find $\Delta g_d = 0.006$ and $\xi = 0.04$, with the term containing $F_d K_d$ in Eq. (4.12) being negligible.

Next we estimate the spin-lattice relaxation rate δ_{sL} from $\xi = \delta_{sL}/\delta_{sf}$, using the modified Overhauser formula[33]

$$\delta_{sf} = 2\pi S(S+1)(\Delta g_s)^2 K_s(\alpha_s)(1-\alpha_s)x/3\hbar\eta_s\,, \tag{4.13}$$

which ignores the effect of d electrons and of magnetic interactions but includes enhancement factors. We assume that this formula is not structure sensitive, i.e., that it applies equally well to amorphous and crystalline systems independent of concentration. This is made plausible by the detailed balance condition[33] $\chi_f \delta_{fs} = \chi_s \delta_{sf}$, where χ_f and χ_s are the Gd and conduction electron susceptibilities, respectively, and δ_{fs} is given by the Korringa relation; for according to this condition, if χ_f, χ_s, and δ_{fs} are not structure sensitive, δ_{sf} should not be, either.

Using $\xi = 0.04$ and Eq. (4.13) with previously given values for K_s, α_s, and η_s, we find $\delta_{sL} \sim 10^{13}$ Hz per atom fraction Gd for our amorphous GdAl system. (If we had used Chock's value for η_s, we would have obtained a value 5 times larger). This result compares remarkably well to the spin-lattice relaxation rates for the dilute crystalline systems $LaAl_2$, YAl_2, and $LuAl_2$, which range from 1×10^{13} to 6×10^{13} Hz per atom fraction Gd.[28,32,33] The order-of-magnitude agreement is plausible because the disorder of random Gd impurities in crystals is qualitatively similar to that in concentrated amorphous systems, and so the spin-flip scattering per Gd atom arising from the disorder should be similar. This point still needs to be verified theoretically, for example, by application of Helman's theory to our case.[35] Our determina-

tion of the spin-lattice relaxation time in amorphous GdAl is one of the first in an amorphous system, the only related earlier work of which we are aware being on liquid lithium, sodium, and potassium by conduction electron spin resonance.[36-38]

The value of Δg_s used in the above analysis implies an sf exchange interaction J_{sf} according to the formula $\Delta g_s = J_{sf}\eta_s/(1-\alpha_s)$, which is a generalization of Eq. (4.9) to include the effect of electron-electron interactions. Using η_s according to Davidov *et al.*[28] one finds $J_{sf} \sim 0.1$ eV, which is a factor of 2 smaller than the values from magnetic measurements discussed earlier. Using η_s according to Chock *et al.*[34] one finds $J_{sf} \sim 0.5$ eV, which is larger than the values from magnetic measurements. Such discrepancies are perhaps not very surprising since the RKKY theory is generally found to give the correct functional form of the magnetic interactions but often fails quantitatively to explain experimental results. Furthermore the above values come from measurements of dilute crystalline systems, and our analysis does not allow us to obtain an independent spin-resonance value for J_{sf} in the amorphous case. Clearly measurements in a lower Gd- concentration range would be of interest to open the bottleneck and make possible such a direct measurement.

Such a measurement would be of particular importance since our resonance value $\Delta g_d = 0.006$, implying a positive J_{df}, contrasts with the result[4] for crystalline $GdAl_2$ of $\Delta g = -0.01$, implying a negative J_{df}. From this change one might be led to conclude that the amorphous structure can have a drastic effect on the exchange interactions. Yet the relative independence of J_{sf} on structure, as deduced from magnetic measurements, indicates the opposite. One may rationalize the situation by speculating that because of their lower symmetry d electrons are more sensitive to structure than s electrons. Furthermore theory[17] indicates that J_{sf} consists of two contributions, one arising from the direct-exchange interaction and being inherently positive, and the other arising from conduction-electron interactions with virtual bound states and being usually negative. We speculate that the balance of these two effects might be very close for d electrons and thus J_{df} could be tipped from positive to negative by structural changes. Unfortunately a detailed theory of such effects appears to be lacking at present.

Finally we turn to the g shifts at lower temperatures, where, as shown in Fig. 7, a rapid increase in g value sets in, attaining values up to $g = 4.5$ at the lowest temperatures. We can compare the size of these shifts to those of crystalline $GdAl_2$,[3,4,39] or of dilute Gd in $LaAl_2$, YAl_2, and $LuAl_2$,[28,32,33] where the maximum shift is only 0.11. A vast host of other Gd-containing systems has been reviewed by Taylor,[40] and the g shifts are usually temperature independent and no larger than a few tenths.[40,41] These shifts are all clearly smaller than our observed low-temperature effect, indicating that our effect cannot be explained in terms of conduction-electron polarization as in Eq. (4.9). A more recent interesting case[42] is that of $La_{3-x}S_4$:Gd where at low temperatures conventional Korringa behavior is observed with a g shift of up to 0.03, but at somewhat higher temperatures a non-Korringa-like linewidth is observed and simultaneously the g shift goes through a peak with temperature, attaining a value of 0.4. This effect was attributed to an excited bound state of $5d$ character which becomes thermally populated at higher temperatures. The effect differs from ours in its temperature dependence. In summary we can find no precedent among Gd-containing systems for the large g shifts we observe at low temperatures. For these reasons we have posited in Eqs. (3.9) and (3.10) the existence of an additional anisotropy field, which is somehow connected to the phenomenon of spin glass ordering in this material, but which has nothing to do with the small intrinsic g shifts we have been considering in this section. In Sec. V we propose a theory for this anisotropy field.

V. INTERPRETATION OF LOW-TEMPERATURE BEHAVIOR

In this section we elaborate on an explanation proposed earlier[11] for the shifts of the resonance to lower fields with decreasing temperature shown in Fig. 3. While the basic features of the explanation remain the same as before, we describe here two aspects not previously covered: (i) We derive the range $2\pi\Lambda_0$ of the exchange interaction. (ii) We discuss the composition dependence of the field shift. Such field shifts have been observed before in other inhomogeneous magnetic systems, in particular CuMn,[43-46] and the relationship of our results with these earlier results has been discussed in Ref. 11.

Two kinds of experiments, namely specific heat[9] and small-angle x-ray scattering[10] have suggested that there exists some kind of magnetic or structural inhomogeneity on a scale of 35 Å in the GdAl amorphous films. We presume that this inhomogeneity consists of regions or clusters in which there is a predominance of ferromagnetic interactions imbedded in an environment with more competing (i.e., ferromagnetic *and* antiferromagnetic) interactions. The clusters could arise ei-

FIG. 9. Schematic inhomogeneous magnetic medium in applied field H. Enclosed shapes represent regions of high susceptibility. Intervening regions are also magnetic but show less net magnetization because of competing ferromagnetic and antiferromagnetic interactions. Needles oriented in the field direction respond most strongly to the applied field.

ther from a locally increased Gd concentration, or else from a configurational order in which, because of statistical randomness, the Gd-Gd near-neighbor distances tend to be less than the average (see Fig. 8). Statistically, these regions will have a variety of shapes—spherical, probate, oblate, as illustrated in Fig. 9.

Consider the magnetic system at a temperature near to, but above, the spin-glass ordering temperature so that the incipiently ferromagnetic regions have a high susceptibility χ. As argued earlier,[11] those regions which are needle-like pointing along the applied-field direction will magnetize most strongly because of their low demagnetizing factor. Other regions, either spherical or needlelike but pointing perpendicular to the applied field, will magnetize much less because of their larger demagnetizing factor. For example consider ellipsoids of revolution with their axis along the field direction and described by a demagnetizing factor D ranging from 0 for a needle to 4π for a pancake. The magnetization M is given by $\chi H/(1+D\chi)$, so that if $\chi \gg 1$, it requires only a small change of D from 0 to $D > \chi^{-1}$ to cause M to drop from χH toward H/D. The regions between the incipiently ferromagnetic regions also magnetize weakly because of the competing exchange interactions. Thus as shown in Fig. 9, one can visualize the magnetic distribution of the inhomogeneous medium as needlelike regions of strong magnetization oriented along the applied field in a matrix of nonuniform but generally weaker magnetization. The axis of the magnetized needles follows the applied dc field, as also shown in Fig. 9, and for different field orientations, the needles which are magnetized are different.

Next we describe a very simplified but explicit calculation for the microwave resonant response of such a system. We use a micromagnetic model and approximate the magnetization M and the exchange stiffness A by

$$M(x,y) = M_0 + M_1 \sin kx \sin ky\,, \tag{5.1}$$

$$A(x,y) = A_0 + A_1 \sin kx \sin ky\,. \tag{5.2}$$

Here M_1 and A_1 are constants describing the magnetic distribution, and we assume M_1 and A_1 are are small compared to M_0 and A_0. Such a magnetic distribution is a checkerboard-type columnar distribution with a periodicity d described by the wave vector $k = 2\pi/d$.[47] Thus it is a simple case of the needlelike magnetization distribution inferred for our material in the previous paragraph. Further we consider the case that the dc magnetic field H_0 lies along the z axis normal to the plane of the film and along the columnar axis, and we assume the film thickness is large compared to the columnar periodicity.

Next we assume that the resonant response of the system to a spatially uniform microwave excitation in the plane of the film has the form

$$\theta = \theta_0 + \theta_1 \sin kx \sin ky\,, \tag{5.3}$$

$$\phi = \omega t\,, \tag{5.4}$$

where θ and ϕ are the conventional polar coordinates relative to the z direction, ω is the angular microwave frequency, and θ_0 and θ_1 are constants describing a nonuniform precessional mode. It can be shown that spatial variation of the phase angle ϕ can be ignored in lowest order. We make one further key assumption, namely, that during the precession, the magnitude of the local magnetization $M(x,y)$ is preserved, i.e., the relaxation rate of $|M(x,y)|$ is small compared to the precession frequency.

As shown in the Appendix, consideration of demagnetizing, applied field, and exchange energies, along with use of the Landau-Lifshitz equations, then leads to the relations

$$\omega\gamma^{-1} = H_0 - 4\pi M_0 + H_{\rm loc}\,, \tag{5.5}$$

$$\theta_1/\theta_0 = -(M_1/M_0)(1+\eta^{-1})^{-1}\,, \tag{5.6}$$

where

$$H_{\rm loc} = (\pi M_1^2/2M_0)(1+\eta^{-1})^{-1}\,, \tag{5.7}$$

$$\eta = (2k\Lambda_0)^2 = (4\pi\Lambda_0/d)^2\,, \tag{5.8}$$

$$\Lambda_0 = (A_0/2\pi M_0^2)^{1/2}\,. \tag{5.9}$$

Next we discuss the physical significance of these results. Equation (5.5) shows that the resonance frequency is shifted from that which would occur in a uniform magnetic system. The field shift $H_{\rm loc}$ (Eq. 5.7) is proportional to the square of the magnetization nonuniformity M_1. The origin of this field shift can be seen from Fig. 10 which shows schematically the resonance mode in the inhomogeneous medium. In the limit of strong exchange coupling between the magnetizations, one may expect all the magnetization to precess at the same angle θ_0 (i.e., $\theta_1 \to 0$). In this case the in-plane component of the magnetization $M(x,y)\sin\theta$ is non-

FIG. 10. Schematic precession modes of an inhomogeneous columnar magnetic system. The columnar axis is assumed to be vertical. In the strong-coupled limit, exchange, represented by the springs, holds precession cone angles constant. The spatially varying magnitude of the magnetization then leads to varying horizontal components and localized magnetic charge, as indicated schematically. This is the origin of the local anisotropy energy. In the weak-coupled limit, exchange is weak and the precession cone angles can adjust to make the horizontal magnetic components constant, thus reducing the anisotropy energy.

uniform and gives rise to in-plane demagnetizing fields H_d which, for a columnar magnetization distribution, are just $2\pi[M(x,y)-M_0]\sin\theta$, where 2π is the demagnetizing factor of a column. This implies a demagnetizing energy $\frac{1}{2}H_dM_p$, where $M_p = [M(x,y)-M_0]\sin\theta$. This energy has the form of a uniaxial anisotropy $K_u\sin^2\theta$ and thus gives rise to the effective anisotropy field $H_{1oc}=2K_u/M_0$, [28]

$$H_{1oc}=2\pi\langle|M(x,y)-M_0|^2\rangle/M_0. \tag{5.10}$$

Here $\langle\ \rangle$ represents a spatial average. Equation (5.10) reduces to Eq. (5.7) if $\eta\to\infty$ and the magnetization of Eq. (5.1) is substituted.

If the exchange coupling is weak, then the opposite limit pertains, as illustrated in Fig. 10. The in-plane demagnetizing energy can be reduced if θ varies spatially, in particular if θ is smaller in those regions where M is larger and vice versa. The criterion for weak or strong exchange coupling is determined by the parameter η in Eq. (5.8). η is determined by the ratio of the length $\Lambda_0=(A_0/2\pi M_0^2)^{1/2}$ to the period $d=2\pi/k$ of the magnetization inhomogeneities. Thus Λ_0 is large if exchange is large and vice versa. Λ_0 is a common parameter in micromagnetic theory and represents the range over which exchange holds spin angles constant against perturbing demagnetizing torques. Thus if $2\pi\Lambda_0>d/2$ ($\eta>1$), that is, if the range $2\pi\Lambda_0$ exceeds the width of one column $\frac{1}{2}d$, the strong-exchange-coupling limit prevails and the field shift is primarily determined by demagnetizing energy.

It must be noted that in the limit of weak exchange coupling ($\eta\ll1$), our derivation is invalid because the system cannot be considered to be described by the single-resonance mode of Eqs. (5.3) and (5.4). Instead each region precesses quasi-independently. Thus our derivation serves chiefly to determine the criterion ($\eta>1$) for the validity of the strong-coupled limit. The range parameter $2\pi\Lambda_0$ may be estimated from formulas for the average exchange stiffness[18]

$$A_0=\tfrac{1}{6}NJS^2x^2zr^2, \tag{5.11}$$

the average magnetization

$$M_0=gS\mu_B xN, \tag{5.12}$$

and the Curie temperature in the molecular-field model

$$kT_C=\tfrac{2}{3}zxS_0(S_0+1)J. \tag{5.13}$$

Here N is the number of atoms per unit volume, J is the average Gd-Gd exchange constant (defined as $E_{ij}=-2JS_iS_j$), S is the average temperature- and field-dependent Gd spin value, S_0 is the zero-temperature value of S ($=\frac{7}{2}$), x is the atom fraction of Gd, z is the average number of nearest neighbors, r is the Gd-Gd interatomic distance, g is the g factor, μ_B is the Bohr magneton, and k is Boltzmann's constant. Of course formulas (5.11)–(5.13) pertain only to a uniform ferromagnetic medium. However since both A_0 and M_0^2 go as S^2, spatial variations in S drop out of the calculation for $\Lambda_0=(A_0/2\pi M_0^2)^{1/2}$, and therefore Eqs. (5.11)–(5.13) can also be used in first approximation for calculating Λ_0 in the inhomogeneous medium.

Taking the atomic volumes Gd (33 Å^3), Al(16.6 Å^3), Ar (53.4 Å^3), and Mo (15.4 Å^3) and adding an additional 5% to account for the typical volume expansion of an amorphous material,[19] we arrive at the values for N and hence $2\pi\Lambda_0$ given in Table I. As mentioned earlier, evidence for inhomogeneities with a dimension of approximately 35 Å has been obtained from specific-heat and small-angle x-ray scattering measurements on the $Gd_{37}Al_{63}$ material. Since the values of $2\pi\Lambda_0$ are equal to or larger than 35 Å in all the samples, it appears that the strong-coupled limit is at least approximately valid.

Assuming the strong-coupled limit, one can now extend the theory for H_{1oc} by using Eq. (5.10) and taking M_0 to be the spatial average $\langle M\rangle$ of an arbitrary magnetization $M(x,y)$. That is, we relax the condition $M_1\ll M_0$ used in deriving Eqs. (5.5)–(5.9). For example in the idealized case where the columnar ferromagnetic regions have magnetization M_1 and occupy volume fraction V_1 of the sample, while the remainder of the sample has magnetization M_2, one finds

$$H_{1oc}=2\pi V_1(1-V_1)(M_1-M_2)^2/\langle M\rangle, \tag{5.14}$$

$$\langle M\rangle=(M_1-M_2)V_1+M_2. \tag{5.15}$$

It is important to recognize that H_{1oc} arises from an anisotropy which is field induced and whose axis therefore follows the direction of the average dc internal field in the sample. In particular, for applied field either perpendicular to or parallel to

the plane of the film, the induced-anisotropy field lies along the same respective directions. Therefore one can simply add H_{loc} to H wherever H appears in the resonance Eqs. (3.3) and (3.4), and thus one obtains Eqs. (3.9) and (3.10). $H_{loc\parallel}$ and $H_{loc\perp}$, the local fields in the parallel and perpendicular configurations, will in general be different. Their size depends on the magnitude of the average internal fields which induce the columnar magnetization, and these internal fields $H_\perp - 4\pi M_\perp$ and $H_\parallel$ are in general not the same. Furthermore there is the possibility of structural anisotropy, for example a preponderance of the needles of Fig. 9 being oriented perpendicular to, rather than parallel to, the film plane. In this case $H_{loc\perp}$ would exceed $H_{loc\parallel}$.

The values of $H_{loc\parallel}$ and $H_{loc\perp}$ for the three samples are shown in Fig. 3. The overall magnitude of H_{loc} is largest for the sample $Gd_{37}Al_{63}$ and decreases to zero in $Gd_{81}Al_{19}$. According to Eq. (5.1), the degree of inhomogeneity must therefore be decreasing as the amount of Gd increases. This agrees with the finding of McGuire *et al.*[8] that as the amount of Gd increases the average magnetic properties of Gd_xAl_{1-x} become more ferromagnetic in character. The interesting point in our work is that the resonance field shift gives a semiquantitative measure of the degree of inhomogeneity and thus aids in characterizing what appears to be a smooth transition between spin-glass behavior and ferromagnetism as a function of composition.

The theoretical prediction for the magnitude of H_{loc} cannot easily be tested because there is insufficient independent knowledge about the nature of the magnetization inhomogeneities. Adopting the simplest possible model of Eqs. (5.14) and (5.15), we can guess that in a spin glass the magnetization of the ferromagnetic regions should be at least as large as the magnetization of the corresponding uniform ferromagnetic material [Eq. (5.12)]. We can also guess that the volume fraction of aligned ferromagnetic needles must be quite small, typically a few percent, since only a small fraction of all the possible shapes are needlelike in any given direction. Working backwards from the observed maximum $H_{loc} = 1900$ Oe and $4\pi M_0 = 850$ G at $T = 12$ K in $Gd_{37}Al_{63}$ [Fig. 3(a)], and taking $4\pi M_1 = 11.5$ kG (the magnetization of the corresponding ferromagnetic material), one predicts $V_1 = 0.03$ and $4\pi M_2 = 600$ G, which are reasonable values. A similar calculation for $Gd_{56}Al_{44}$ at $T = 8$ K yields $H_{loc} = 1500$ Oe, $4\pi M_0 = 7.3$ kG, $4\pi M_1 = 14.5$ kG, $V_1 = 0.3$, and $4\pi M_2 = 4$ kG. In this sample a much larger volume fraction appears to be ferromagnetic.

It is interesting to speculate about the significance of such a gradual transition from spin glass to ferromagnetic behavior. A ferromagnet with domain walls and coercivity exhibits many of the characteristics of a spin glass, for example an average magnetization that can be zero in zero field, a susceptibility peak (net magnetization dropping off at low temperatures because of demagnetization) and thermal remanent effects (because of coercivity). Of course there are quantitative differences but from a qualitative point of view a spin glass may be viewed as a ferromagnet with a very small domain size or a very large number of domain walls. This is particularly true if one does not ignore (as so many theories have done) magnetostatic effects but includes them on an equal footing with exchange interactions in determining the favored magnetic structure. Thus one can visualize a smooth transition between spin glass and ferromagnet as a function of domain size. $Gd_{37}Al_{63}$ apparently falls in this continuum with a domain size of order 35 Å. The gradual homogenization of the magnetization indicated by the magnetic resonance may imply a steady increase in the domain size with Gd concentration. Specific-heat studies or direct microscopic domain observations would be of interest to confirm this hypothesis.

Finally we comment briefly on the linewidth (Fig. 4), intensity (Fig. 5), and remanence (Fig. 6) of the resonance signal. It is not clear if the increase in linewidth at low temperatures is directly related to the shift of the resonance field. Increase in the linewidth is observed near the ordering temperature of many ferromagnets even where there is no field shift. In the context of our strong-coupled model, the linewidth can be attributed to magnetic inhomegeneity on a scale larger than $2\pi\Lambda_0$, because that part of the inhomegeneity which is on a smaller scale and which gives rise to the field shift should be exchange narrowed. The fact that the intensity of the resonance signal (Fig. 5) has a maximum near the susceptibility maximum is reasonable because resonance signals generally increase with the magnetization. We have not yet attempted a quantitative theory of the intensity.

The isothermal remanent effect shown in Fig. 6 follows a logarithmic law. This result is in accord with the theory of Holtzberg, Tholence, and Tournier[48] who treat the behavior of the inhomogeneous magnetic system as a collection of independent magnetic subsystems each with its local anisotropy arising from dipolar interactions. Such a theory is related in concept to our proposed origin for the anisotropy field, although it differs in that we consider a field-induced anisotropy, without which the shift of both $H_\parallel$ and $H_\perp$ would be hard to explain. Another difference is that Holtzberg *et al.* assume the magnetic subsystems are

superparamagnetic above the apparent spin-glass freezing temperature and that there is a distribution of blocking temperatures at which the subsystems freeze. In this case there should still be a substantial remanence at the susceptibility maximum, which, however, is not observed in the GdAl amorphous films.[6-8]

In conclusion, magnetic resonance data, in conjunction with earlier magnetic data, have allowed us to make a detailed test of the RKKY theory in an amorphous alloy and to follow for the first time the evolution of local anisotropy fields of an inhomogeneous magnetic system in a transition from spin-glass to ferromagnetic behavior.

ACKNOWLEDGMENTS

The authors thank P. Chaudhari for initially suggesting the experiment, R. J. Gambino for the samples, H. Lilienthal for the magnetic measurements, G. A. Corker for the use of the Varian resonance spectrometer, and G. S. Cargill, J. M. D. Coey, B. Elschner, M. Freiser, R. J. Gambino, S. Hart, S. Kirkpatrick, A. Meyer, T. R. McGuire, T. Mizoguchi, P. Monod, J. C. Slonczewski, R. Tournier, S. von Molnar, and P. Wigen for valuable discussions.

APPENDIX: DERIVATION OF RESONANCE MODE IN AN INHOMOGENEOUS SYSTEM

We consider the checkerboard columnar magnetic system described by the spatially sinusoidally varying magnetization $M(x,y)$ of Eq. (5.1) and exchange stiffness $A(x,y)$ of Eq. (5.2). A dc field H_0 is applied along the z axis perpendicular to the film plane. The periodicity $d=2\pi/k$ of the columnar structure is much smaller than the film thickness. We seek to determine the resonant response of such a system to microwave excitation. We use a perturbation approach and assume the response will be described by Eqs. (5.3) and (5.4), i.e., by the angular resonance frequency ω and the spatial variation of the precession amplitude θ_1/θ_0.

The motion is governed by the Landau-Lifshitz equations:

$$d\theta/dt = -\gamma(M\sin\theta)^{-1}\delta w/\delta\phi\,, \tag{A1}$$

$$d\phi/dt = \gamma(M\sin\theta)^{-1}\delta w/\delta\theta\,, \tag{A2}$$

where γ is the gyromagnetic ratio, M the local magnetization as in Eq. (5.1), and w the local static-energy density. To solve these equations we write a variational form[49] of Eqs. (A1) and (A2)

$$\delta w = (\delta w/\delta\phi)\delta\phi + (\delta w/\delta\theta)\delta\theta\,. \tag{A3}$$

Substituting Eq. (A1) and (A2) for $\delta w/\delta\phi$ and $\delta w/\delta\theta$, integrating over space and differentiating with respect to the dynamical variables X_i, one obtains

$$\int dV\frac{\delta w}{\delta X_i} = \int dV\left[\left(-M\gamma^{-1}\sin\theta\frac{d\theta}{dt}\right)\left(\frac{\delta\phi}{\delta X_i}\right) + \left(M\gamma^{-1}\sin\theta\frac{d\phi}{dt}\right)\left(\frac{\delta\theta}{\delta X_i}\right)\right]. \tag{A4}$$

Here we interpret θ_0 and θ_1 to be the dynamical variables X_i. Since $\delta\phi/\delta X_i = 0$ and $d\phi/dt = \omega$ according to Eqs. (5.4), the equations simplify to

$$\int dV\frac{\delta w}{\delta\theta_0} = \omega\gamma^{-1}\int dVM\sin\theta\,, \tag{A5}$$

$$\int dV\frac{\delta w}{\delta\theta_1} = \omega\gamma^{-1}\int dVM\sin\theta\sin kx\sin ky\,. \tag{A6}$$

Next we evaluate w, which is comprised of magnetostatic, field, and exchange terms. The magnetostatic contribution has two parts, one arising from the in-plane components of the precessing magnetization and the other arising from the average demagnetizing field along the z direction. As described by Cargill and Mizoguchi,[47] the in-plane part gives rise to an energy

$$V^{-1}\int dVw_{mp} = \pi V^{-1}\int dV(M_p - M_{p\,\mathrm{av}})^2\,, \tag{A7}$$

where

$$M_p = M_0\theta_0 + (M_0\theta_1 + M_1\theta_0)\sin kx\sin ky \tag{A8}$$

is the in-plane component of the magnetization and

$$M_{p\,\mathrm{av}} = V^{-1}\int dVM_p = M_0\theta_0 \tag{A9}$$

is the spatially averaged in-plane component. Here we have assumed θ_0 and θ_1 are both small and have kept terms to first order only. Thus one finds

$$V^{-1}\int dVw_{mp} = (\tfrac{1}{4}\pi)(M_1\theta_0 + \theta_1 M_0)^2\,. \tag{A10}$$

The other magnetostatic contribution, arising from the average demagnetizing field in the z direction, is

$$V^{-1}\int dVw_{mn} = V^{-1}\int dV2\pi M_n M_{n\,\mathrm{av}}\,, \tag{A11}$$

where

$$M_n = (M_0 + M_1\sin kx\sin ky)[1 - \tfrac{1}{2}(\theta_0 + \theta_1\sin kx\sin ky)^2] \tag{A12}$$

is the instantaneous normal magnetization and $M_{n\,\mathrm{av}}$ is its spatial average. Thus one finds

$$V^{-1}\int dV w_{mn} = +2\pi M_0^2(1-\theta_0^2-\tfrac{1}{4}\theta_1^2) - \pi M_0 M_1 \theta_0 \theta_1 . \tag{A13}$$

The field contribution is similarly

$$V^{-1}\int dV w_H = V^{-1}\int dV M_n H_0 = H_0(-M_0 + \tfrac{1}{2}M_0\theta_0^2 + \tfrac{1}{8}M_0\theta_1^2 + \tfrac{1}{4}M_1\theta_0\theta_1) . \tag{A14}$$

The local exchange energy is

$$w_A = A[(\partial\theta/\partial x)^2 + (\partial\theta/dy)^2] \tag{A15}$$

which leads to

$$V^{-1}\int dV w_A = \tfrac{1}{2}\theta_1^2 k^2 A_0 . \tag{A16}$$

It is noteworthy that A_1 drops out of this expression and thus gives no first-order contribution to H_{1oc}. The sum of Eqs. (A10), (A13), (A14), and (A16) gives the total energy. Taking the derivative of these expressions with respect to θ_0 and evaluating the right-hand side of Eq. (A5), one finds

$$\tfrac{1}{2}\pi M_1(M_0\theta_1 + \theta_0 M_1) + (H_0 - 4\pi M_0)(M_0\theta_0 + \tfrac{1}{4}M_1\theta_1) = \omega\gamma^{-1}(M_0\theta_0 + \tfrac{1}{4}M_1\theta_1) . \tag{A17}$$

Proceeding similarly with θ_1 and evaluating the right-hand side of Eq. (A6), one finds

$$\theta_1 k^2 A_0 + \tfrac{1}{4}(H_0 - 2\pi M_0)(M_0\theta_1 + \theta_0 M_1) = \tfrac{1}{4}\omega\gamma^{-1}(M_0\theta_1 + \theta_0 M_1) . \tag{A18}$$

These equations can be solved to give Eqs. (5.5) and (5.6) of Sec. V, which is the result we sought.

*Present address: CNRS, Laboratoire de Physique des Solides, Bâtiment 510, 91405-Orsay, France.

[1]K. N. R. Taylor, Adv. Phys. 20, 551 (1971).

[2]W. E. Wallace, *Rare Earth Intermetallics* (Academic, New York, 1973).

[3]M. Peter, J. Appl. Phys. 32, 338S (1961).

[4]M. Peter, D. Shaltiel, J. H. Wernick, H. J. Williams, J. B. Mock, and R. C. Sherwood, Phys. Rev. 126, 1395 (1962).

[5]D. Shaltiel, J. H. Wernick, H. J. Williams, and M. Peter, Phys. Rev. A 135, 1346 (1964).

[6]T. Mizoguchi, T. R. McGuire, S. Kirkpatrick, and R. J. Gambino, Phys. Rev. Lett. 38, 89 (1977).

[7]T. Mizoguchi, T. R. McGuire, R. J. Gambino, and S. Kirkpatrick, Physics 86–88B, 783 (1977).

[8]T. R. McGuire, T. Mizoguchi, R. J. Gambino, and S. Kirkpatrick, J. Appl. Phys. 49, 1689 (1978).

[9]J. M. D. Coey, S. von Molnar, and R. J. Gambino, Solid State Commun. 24, 167 (1977).

[10]G. S. Cargill III (private communication).

[11]A. P. Malozemoff and J. P. Jamet, Phys. Rev. Lett. 39, 1293 (1977).

[12]G. E. Pake and E. M. Purcell, Phys. Rev. 74, 1184 (1948); G. Feher and A. F. Kip, Phys. Rev. 98, 337 (1955).

[13]R. La Croix, Helv. Phys. Acta 30, 374 (1957).

[14]M. A. Ruderman and C. Kittel, Phys. Rev. 96, 99 (1954).

[15]T. Kasuya, Prog. Theor. Phys. 16, 45 (1956).

[16]K. Yosida, Phys. Rev. 106, 893 (1957).

[17]P. G. deGennes, J. Phys. Radium 23, 510 (1962).

[18]A. Gangulee and R. C. Taylor, J. Appl. Phys. 49, 1762 (1978).

[19]S. J. Poon and J. Durand, Phys. Rev. B 16, 316 (1977).

[20]J. J. Hauser, Phys. Rev. B 12, 5160 (1975).

[21]B. Boucher, J. Phys. Lett. (Paris) 37, L345 (1976).

[22]K. Lee and N. Heiman, AIP Conf. Proc. 24, 108 (1975).

[23]N. Heiman and N. Kazama, J. Appl. Phys. 49, 1686 (1978).

[24]S. J. Poon and J. Durand, Solid State Commun. 21, 793 (1977).

[25]J. Korringa, Physica (Utr.) XVI, 601 (1950).

[26]S. W. Charles, J. Popplewell, and P. A. Bates, J. Phys. F 3, 664 (1974).

[27]D. Davidov, K. Maki, R. Orbach, C. Rettori, and E. P. Chock, Solid State Commun. 12, 621 (1973).

[28]D. Davidov, A. Chelkowski, C. Rettori, R. Orbach, and M. B. Maple, Phys. Rev. B 7, 1029 (1973).

[29]A. Narath and H. T. Weaver, Phys. Rev. 175, 373 (1968).

[30]R. W. Shaw, Jr., and W. W. Warren, Jr., Phys. Rev. B 3, 1562 (1971).

[31]D. Davidov and D. Shaltiel, Phys. Rev. Lett. 21, 1752 (1968).

[32]W. Schäfer, H. K. Schmidt, B. Elschner, and K. H. J. Buschow, Z. Phys. 254, 1 (1972).

[33]C. Rettori, H. M. Kim, E. P. Chock, and D. Davidov, Phys. Rev. B 10, 1826 (1974).

[34]E. P. Chock, R. A. B. Devine, S. A. Dodds, R. Orbach, and L. Tippie, J. Phys. F 7, 1097 (1977).

[35]J. S. Helman, Phys. Kondens. Mater. 6, 297 (1967).

[36]J. R. Asik, M. A. Ball, and C. P. Slichter, Phys. Rev. 181, 645 (1969).

[37]R. A. B. Devine and R. Dupree, Philos. Mag. 21, 789 (1970); 22, 657 (1970).

[38]C. Taupin, M. Lambert, and Ch. Mazieres, J. Phys. Chem. Solids 32, 2045 (1971).

[39]B. R. Coles, D. Griffiths, R. J. Lowin, and R. H. Taylor, J. Phys. C 3, 1121 (1970).

[40]R. H. Taylor, Adv. Phys. 24, 681 (1975).

[41]G. Heinrich and A. Meyer, Solid State Commun. 21, 21 (1977).

[42]D. Stoppels, R. Valkenburg, and G. A. Sawatzky, Phys. Status Solidi B 86–88B, 135 (1977).

[43]H. Nagashima and H. Abe, J. Phys. Soc. Jpn. 32, 1507 (1972).

[44]J. Owen, M. Browne, W. D. Knight, and C. Kittel, Phys. Rev. 102, 1501 (1956); J. Owen, M. Browne, V.

Arp, and A. F. Kip, J. Phys. Chem. Solids 2, 85 (1957).
[45]D. Griffiths, Proc. Phys. Soc. Lond. 90, 707 (1967).
[46]J. S. Kouvel, J. Phys. Chem. Solids 21, 57 (1961); 24, 795 (1963).
[47]G. S. Cargill and T. Mizoguchi, J. Appl. Phys. 49, 1753 (1978).
[48]F. Holtzberg, J. L. Tholence, and R. Tournier, *Amorphous Magnetism* II, edited by R. A. Levy and R. Hasegawa (Plenum, New York, 1976), p. 155.
[49]J. C. Sloncewski, J. Appl. Phys. 45, 2705 (1974).